AD-A138 979 INVERSION OF EXPERIMENTAL OPTICAL DATA(U) BOEING AEROSPACE CO SEATTLE WA C D CAPPS ET AL. FEB 84 CRDC-CR-84018 DAAK11-82-C-0104 1/1

UNCLASSIFIED F/G 20/6 NL

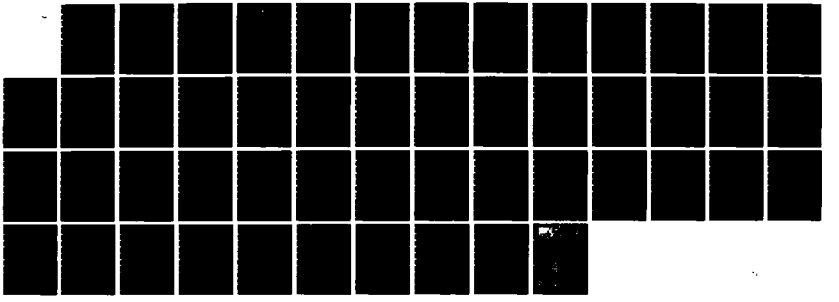

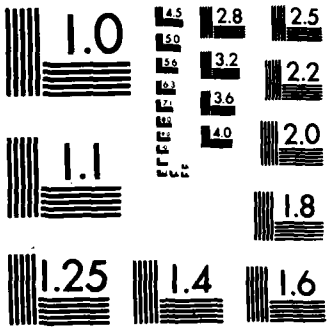

(12)

AD

CRDC-CR-84018

INVERSION OF EXPERIMENTAL OPTICAL DATA

by C. D. Capps
A. R. Tokuda
G. M. Hess

BOEING AEROSPACE COMPANY
P.O. Box 3999
Seattle, Washington 98124

Contract No. DAAK11-82-C-0104

February 1984

US Army Armament, Munitions & Chemical Command
Aberdeen Proving Ground, Maryland 21010

Disclaimer

The findings in this report are not to be construed as an official Department of the Army position unless so designated by other authorizing documents.

Disposition

For classified documents, follow the procedures in DOD 5200.1-R, Chapter IX, or DOD 5220.22-M, "Industrial Security Manual," paragraph 19. For unclassified documents, destroy by any method which precludes reconstruction of the document.

Distribution Statement

Approved for public release; distribution is unlimited.

UNCLASSIFIED

SECURITY CLASSIFICATION OF THIS PAGE (When Data Entered)

REPORT DOCUMENTATION PAGE		READ INSTRUCTIONS BEFORE COMPLETING FORM
1. REPORT NUMBER CRDC-CR-84018	2. GOVT ACCESSION NO. AD-A138979	3. RECIPIENT'S CATALOG NUMBER
4. TITLE (and Subtitle) INVERSION OF EXPERIMENTAL OPTICAL DATA		5. TYPE OF REPORT & PERIOD COVERED Contractor Report 13 Aug 82 - 13 Sep 83
		6. PERFORMING ORG. REPORT NUMBER
7. AUTHOR(s) C. D. Capps A. R. Tokuda G. M. Hess		8. CONTRACT OR GRANT NUMBER(s) DAAK11-82-C-0104
9. PERFORMING ORGANIZATION NAME AND ADDRESS Boeing Aerospace Company PO Box 3999 Seattle, Washington 98124		10. PROGRAM ELEMENT, PROJECT, TASK AREA & WORK UNIT NUMBERS
11. CONTROLLING OFFICE NAME AND ADDRESS Commander, Chemical Research and Development Center ATTN: DRSMC-CLJ-IR (A) Aberdeen Proving Ground, Maryland 21010		12. REPORT DATE February 1984 13. NUMBER OF PAGES 47
14. MONITORING AGENCY NAME & ADDRESS(if different from Controlling Office) Commander, Chemical Research and Development Center ATTN: DRSMC-CLB-PS (A) Aberdeen Proving Ground, Maryland 21010		15. SECURITY CLASS. (of this report) UNCLASSIFIED 15a. DECLASSIFICATION/DOWNGRADING SCHEDULE NA

16. DISTRIBUTION STATEMENT (of this Report)

Approved for public release; distribution is unlimited.

17. DISTRIBUTION STATEMENT (of the abstract entered in Block 20, if different from Report)

18. SUPPLEMENTARY NOTES

Contracting Officer's Representative: Dr. Bottiger (DRSMC-CLB-PS (A))
(301) 671-2395

19. KEY WORDS (Continue on reverse side if necessary and identify by block number)

Inversion
Remote Sensing
Analytic Inversion
Constraints and Inversion

20. ABSTRACT (Continue on reverse side if necessary and identify by block number)

Particle size distributions were obtained by inversion of simulated scattering data using an analytic algorithm. An extension of the analytic inversion technique to incorporate constraints is also presented.

DD FORM 1 JAN 73 1473 EDITION OF 1 NOV 65 IS OBSOLETE

UNCLASSIFIED

SECURITY CLASSIFICATION OF THIS PAGE (When Data Entered)

Blank

PREFACE

The work described in this report was done under Contract No. DAAK11-82-C-0104. This work was started in August 1982 and completed in September 1983.

The use of trade names in this report does not constitute an official endorsement or approval of the use of such commercial hardware or software. This report may not be cited for purposes of advertisement.

This report has been approved for release to the public.

Blank

CONTENTS

LIST OF FIGURES

Blank

INVERSION OF EXPERIMENTAL OPTICAL DATA

1. INTRODUCTION

There exist several inversion techniques for inferring the particle size distributions from scattering measurements done on aerosols composed of spherical particles. This report will treat several areas related to the practical application of inversion algorithms to actual experimental measurements to obtain size distributions.

The first area to be discussed is the one of which measurements to make. Due to the nature of the Mie function which describes the scattering process certain measurements contain more information than others. However, practical considerations, e.g., availability of sources, optics, and detectors, limit what experiments can be done. Optimization of the measurement process under both of these constraints will be discussed in Section 2.

Section 3 presents the data that will be used in the inversion and preliminary analysis. In order to invert the data it is necessary to first estimate the radius range spanned by the particles in the distribution. This is done by fitting the data with a log-normal size distribution and inferring the radius range from the fitted parameters.

In Section 4 an analytic inversion technique will be applied to the simulated experimental data provided by the Chemical Research and Development Center (CRDC) to obtain particle size distributions. This analytic method was developed to provide a better understanding of the inversion process, i.e., how the information content of the measurement set influences the uncertainty in the calculated size distribution. As this was a blind test, i.e. the size distributions were unknown to those doing the inversion, the insights achieved with this method are especially relevant to the practical inversion problem.

Section 5 will discuss an extension of the analytic inversion method in which constraints can be added to improve the inversion and yet

the effects of the data and constraints can be separated quantitatively. Recommendations for future research are made in Section 6.

2. OPTIMIZATION

The technique used to select the optimal measurement set has been described in detail.[1,2] Briefly, the method involves determining the number of independent pieces of information contained in a large set of possible measurements through the use of an eigenanalysis of the measurement covariance matrix. Superfluous measurements are excluded one at a time according to the algorithm until the number of measurements and independent pieces of information are approximately equal. The measurement set with the largest number of independent pieces of information is taken as the optimum as it contains the most information about the range of particle sizes.

Basically, three types of mesurements were examined for particles in the range 0.002 to 2.6 microns in diameter. These were intensity in the backscatter direction at different wavelengths, intensity at one wavelength over a range of scattering angles in the near forward direction, and polarization at one wavelength over the full range of scattering angles. The optimal set was found to be wavelength dependence of the intensity in the backscatter direction. These wavelengths are listed in Table 1.

Table 1. Optimal Wavelength Set

Kernel Index	Wavelength (microns)
1	0.266
2	0.524
3	0.782
4	1.04
5	1.55
6	2.33
7	2.59
8	2.85
9	3.63
10	3.88
11	4.14
12	4.91

It must be recognized that this set is based on a limited search. The search region should be broadened considerably in order to confidently establish an optimum measurement set.

Two explicit suggestions can be made in regard to this search; the wavelength of 0.266 micron is not practical for field measurements and should not be included in a real set, and the range of particles sizes should be increased so that the upper limit on diameter is approximately 10 microns. Futher recommendations will be made in Section 6.

3. PRELIMINARY DATA ANALYSIS

The system modeled for this simulated experiment was a polydisperse hydrosol of polystyrene latex spheres. Five distribution functions, known only to the Chemical Research and Development Center, were used to create the five synthetic data sets labeled by the letters "A" through "E". These sets were created by multiplying a distribution function by the total and differential cross sections given by Mie theory for 15 different wavelengths and integrating over particle radius. In order to simulate actual experiments a random error with a known variance was added to each data item. Each of the five data sets then consisted of the total and differential cross sections at 15 wavelengths with the error included. Table 2 lists the wavelengths in the water medium and the latex/water relative refractive indices used.

Table 2. Optical Parameters

Wavelength in Water (microns)	Relative Refractive Index
0.222	1.2563
0.266	1.2275
0.524	1.1900
0.782	1.1861
1.04	1.1889
1.55	1.2017
2.33	1.3397
2.59	1.1330
2.85	1.1529
3.63	1.1779
3.88	1.1859
4.14	1.2005
4.91	1.1725
6.20	1.2133
8.99	1.3286

As discussed in Section 2 the optimum measurements are the backscatter cross sections at the wavelengths given in Table 1. These are included in the CRDC data sets. Therefore, the inversion work presented in this report will use the backscatter cross sections listed in Table 3 as its basic data.

Table 3. Backscatter Cross Section (Micron^2)

Wavelength	Set A	Set B	Set C	Set D	Set E
0.222	9.13	9.95	4.01	15.7	3.08
0.266	12.6	15.9	5.78	19.0	2.68
0.524	6.27	6.66	8.36	26.0	1.81
0.782	1.72	1.68	4.75	8.93	.602
1.04	.831	.856	2.42	4.24	.294
1.55	.463	.555	.924	1.69	.179
2.33	2.10	2.61	2.69	4.88	.490
2.59	.109	.143	.0788	.182	.0292
2.85	.168	.194	.101	.295	.0417
3.63	.242	.344	.117	.529	.0645
3.88	.262	.361	.142	.626	.0711
4.14	.319	.444	.182	.822	.0863
4.91	.184	.195	.126	.475	.0541
6.20	.260	.300	.257	.752	.0751
8.99	.554	.644	.507	1.39	.119
Fractional Error	.03	.10	.03	.03	.03

The first step in the analysis of the data is to determine the size range of the particles present in the distribution. This is necessary for two reasons. In order to numerically integrate over the rapidly oscillating Mie cross section it is necessary to have a large number of integration points per radius interval; approximately 400 points per micron for 0.10% accuracy for the wavelengths listed in Table 3. Computation time is, therefore, significantly increased if a larger than required radius interval is used. Secondly, the backscatter cross section is essentially the product of a function that oscillates about an equilibrium value and the radius squared. If larger radii than needed are included sensitivity to the smaller, significant radius values is reduced. This is easily seen in Figure 3 of the second literature cited. The portion of the distribution function that is recoverable by inversion is a linear combination of functions of the form plotted in that figure. As none of the functions shown have significant values for radii less than about 0.4 microns it would be impossible to construct a distribution function that had its major contribution in this region. Thus, it is important both for theoretical and practical reasons to bound the radius region before an inversion is done.

This was accomplished by first fitting the data with a log-normal particle size distribution which has the form

$$f(r) = \frac{N}{r \ln s \quad 2\pi} \exp \quad - \frac{1}{2} \left(\frac{\ln 2r - \ln D}{\ln s}\right)^2 \qquad (1)$$

where N = total number of particles
D = geometric mean diameter
s = geometric standard deviation.

The rationale for this function is that it is found in many natural particle size distributions involving condensation phenomena and that it is significant in only a limited region. The predicted backscatter cross section σ_p (λ, N, D, s) is given by

$$\sigma_p(\lambda, N, D, s) = \int_0^5 \sigma_m(r, \lambda)\, f(r)\, dr \qquad (2)$$

where λ = wavelength

σ_m = Mie theory backscatter cross section.

The upper limit of 5 microns in the integral was provided by CRDC. In a real problem this upper limit would have to be determined by physical considerations, such as settling rates. The parameters N, D, and s were estimated by using a Marquardt-Levenberg[3] algorithm to minimize chi-square for each data set. Chi-square is defined as

$$\chi^2 = \sum_{\lambda} \left(\frac{\sigma(\lambda) - \sigma_p(\lambda)}{e\ \sigma(\lambda)}\right)^2$$

where $\sigma(\lambda)$ are the backscatter cross sections and c is the fractional uncertainty listed in Table 3. The resulting parameter values are given in Table 4 and the corresponding plots of f(r) in Figures 1-5.

Table 4. Values From Log-Normal Fit

Set	Number of Particles	Geometric Mean Diameter (Micron)	Geometric Standard Derivation
A	0.829	2.85	1.40
B	0.959	3.03	1.33
C	0.579	1.61	5.56
D	0.745	4.33	1.36
E	1.03	0.952	2.07

Even if the actual distribution is not a log-normal the above fitting procedure should produce useful information about the range of particle sizes. For example, if the actual size distribution were bimodal the fit could place the single log-normal peak at an intermediate position and increase the width to include the significant portion of the distribution. The radius range used in the inversion was the region that included 99% of

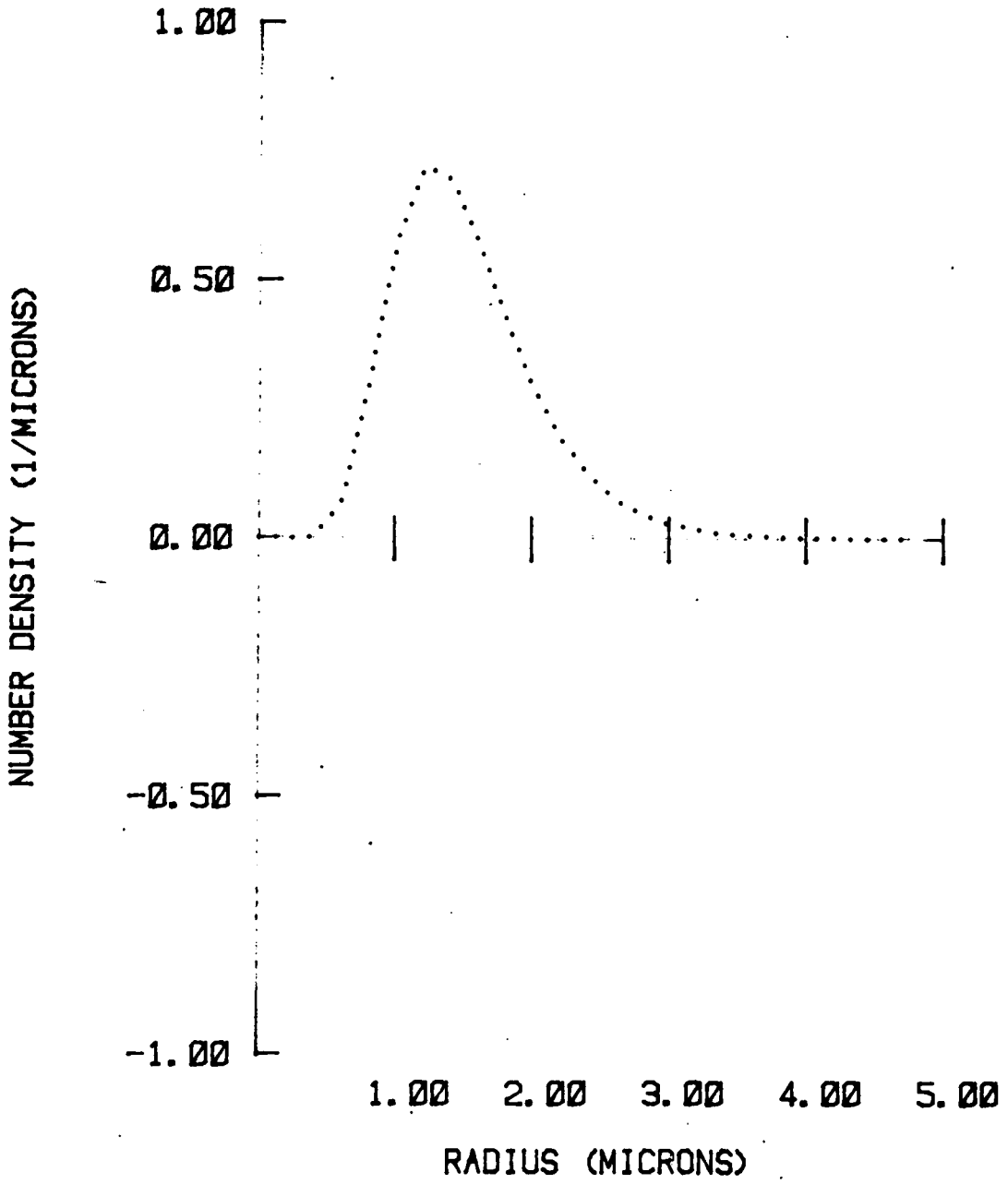

Figure 1. Log-normal Size Distribution Fit to Set A

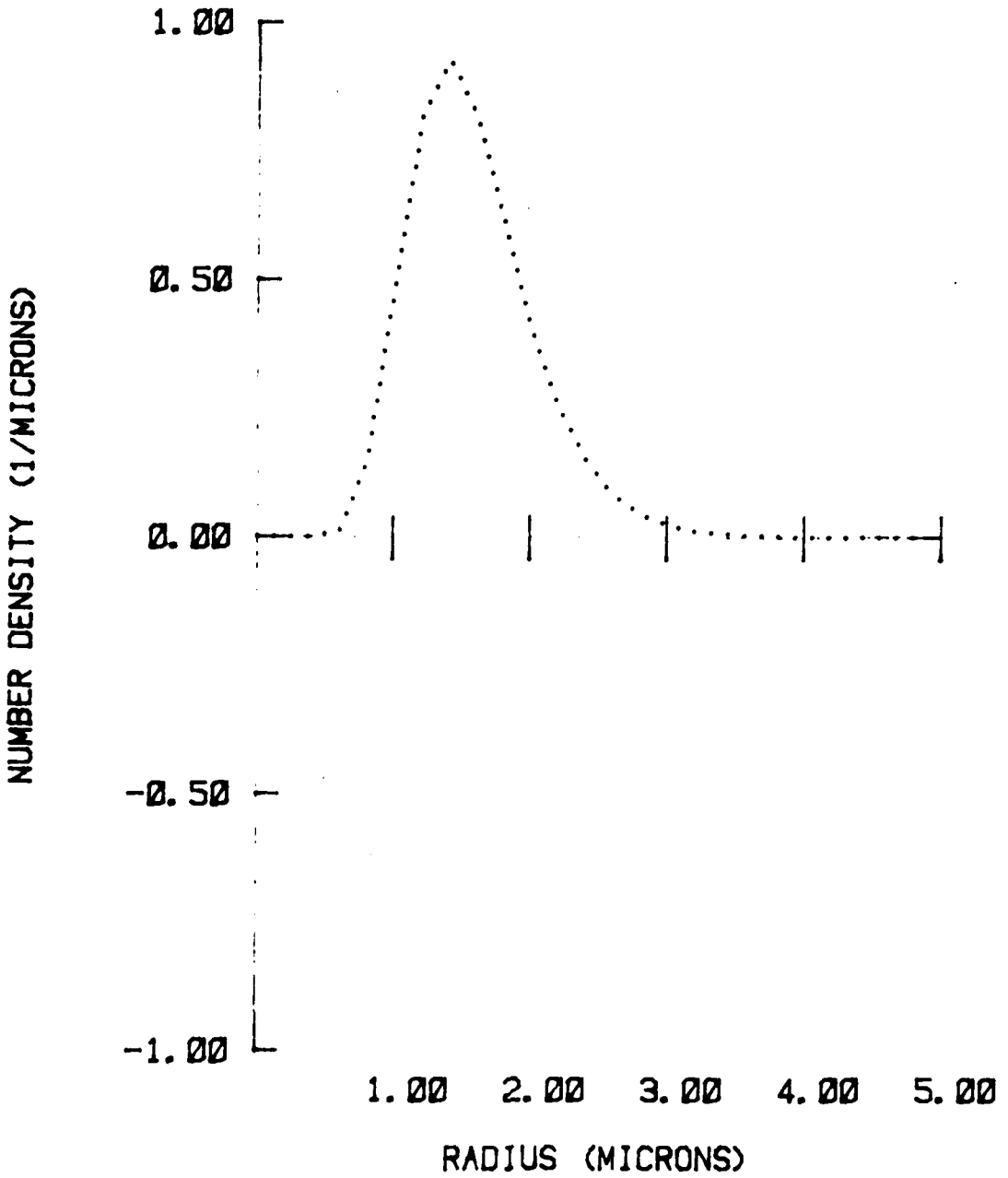

2. Log-normal Size Distribution Fit to Set B

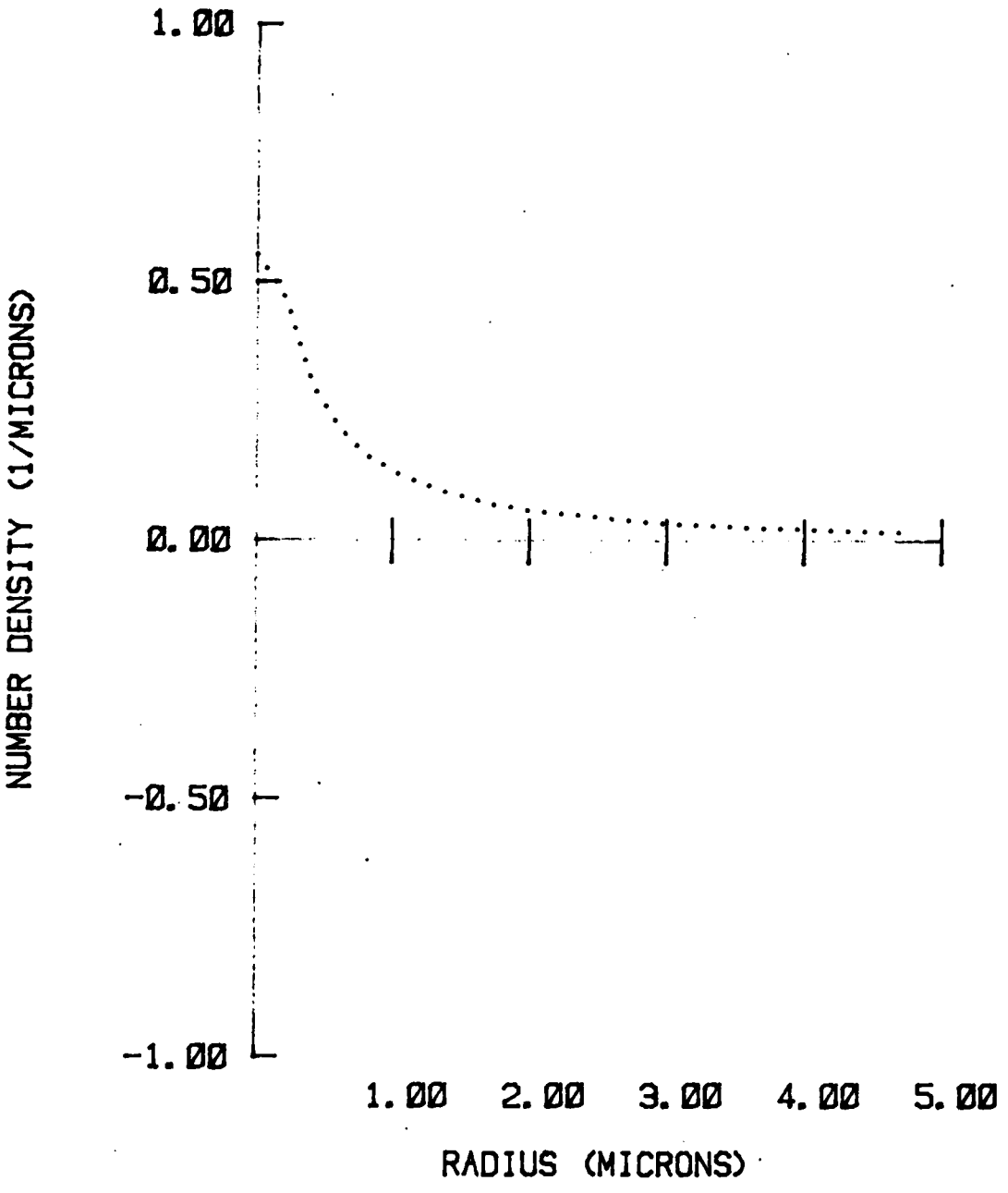

Figure 3. Log-normal Size Distribution Fit to Set C

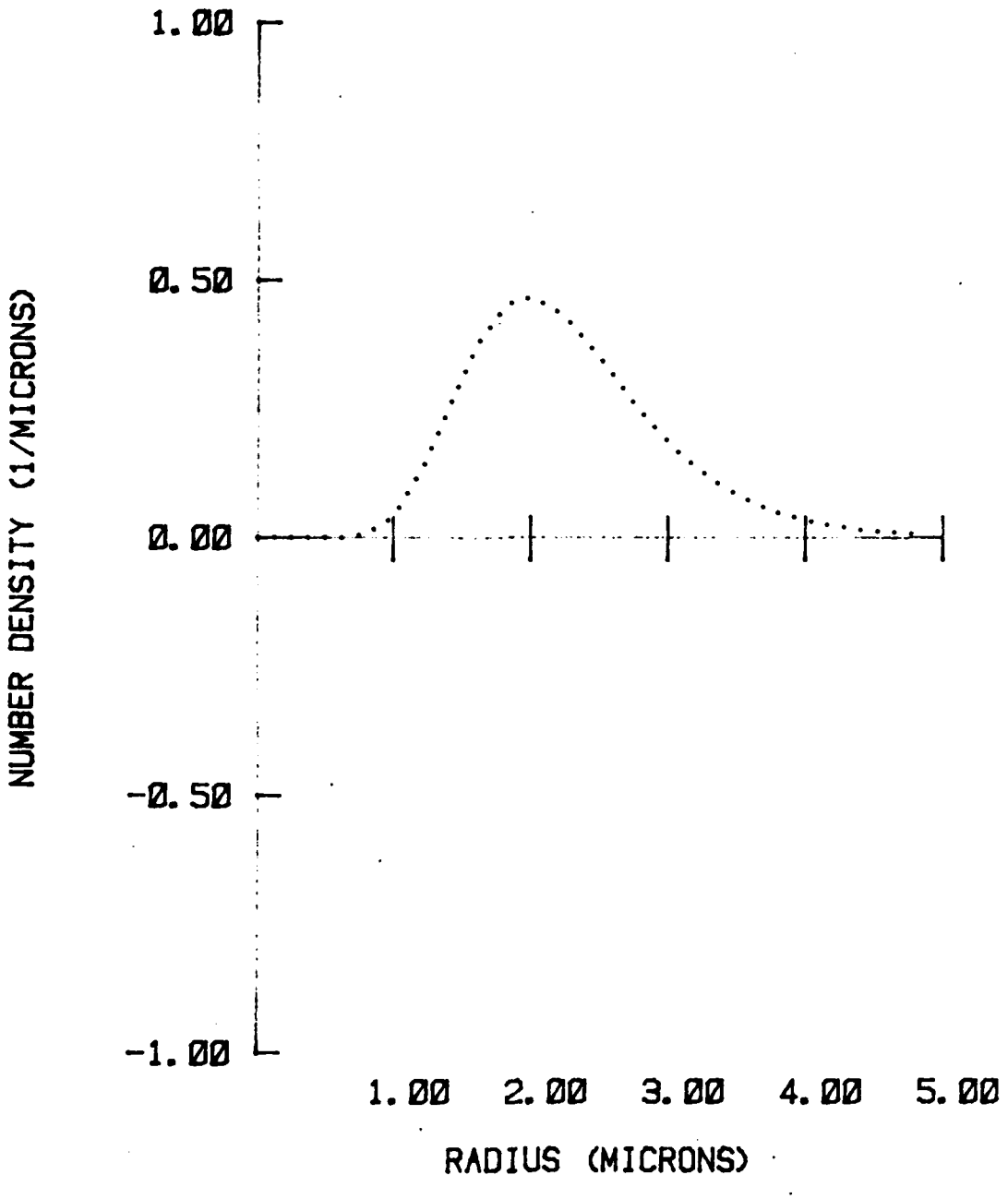

Figure 4. Log-normal Size Distribution Fit to Set D

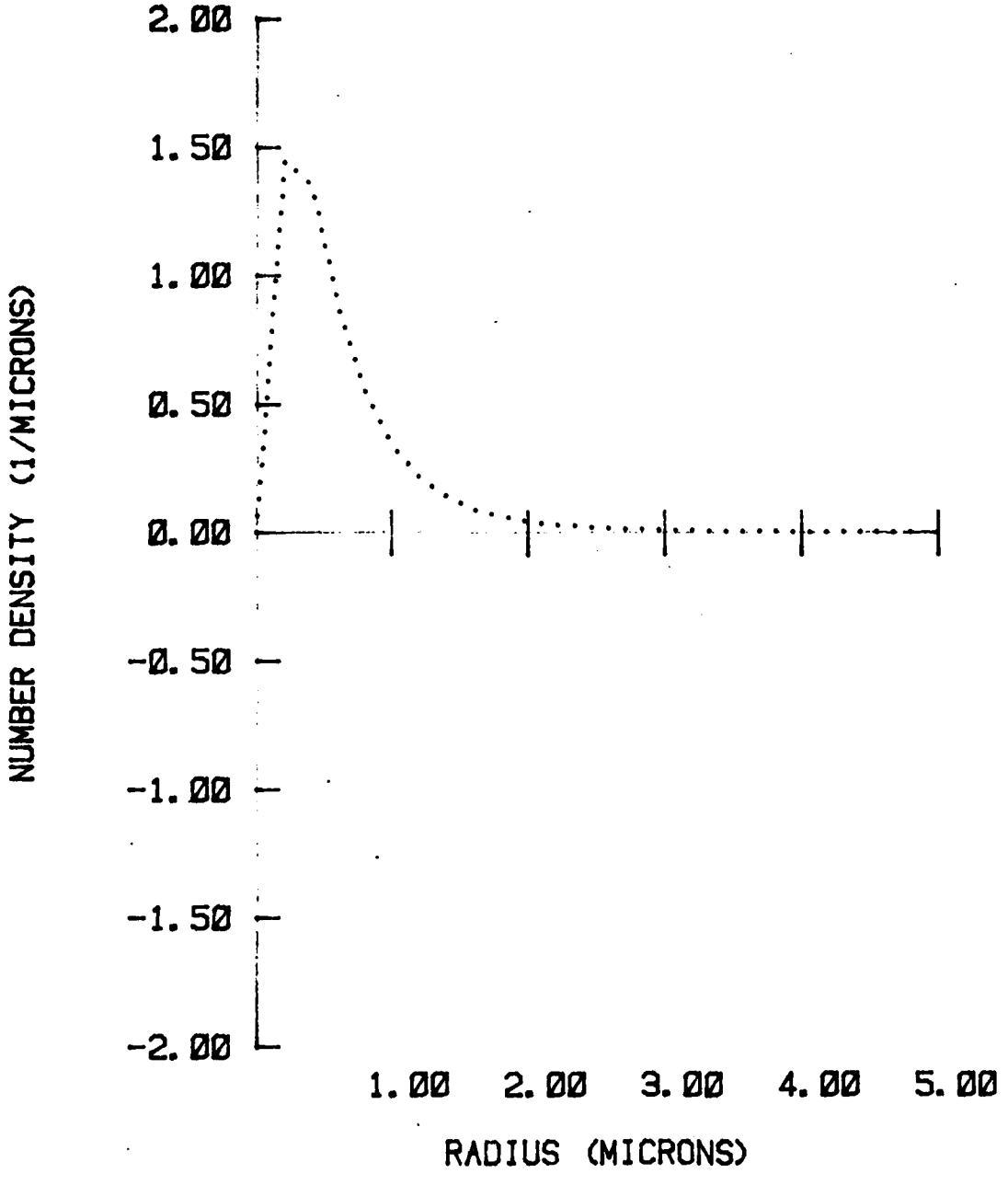

Figure 5. Log-normal Size Distribution Fit to Set E

the area under the distribution f(r). The upper and lower limits on r are calculated from the fit parameters D and s

$$r_{\pm} = \left(\frac{D}{2}\right) s^{\pm 2.6} \tag{4}$$

and are listed in Table 5.

Table 5. Radius Region Used for Inversion

Set	Minimum Radius (Microns)	Maxium Radius (Microns)
A	.59	3.42
B	.72	3.18
C	.03	5.00*
D	.98	4.83
E	.07	3.15

*Defined upper limit

4. INVERSION RESULTS

The data were inverted using the analytic inversion method.[1,2] This method returns only that portion of the solution that depends on the data and the Mie cross section; i.e. it makes no assumptions regarding functional form or smoothness of the size distribution. The inversions were performed in the radius intervals specified in Table 5 and the results plotted in Figures 6 through 10 where the number density for both the log-normal fit and inversion result are shown. Figures 11 through 15 give the corresponding volume density plots where the volume density g is defined as

$$g(r) = \frac{4}{3} \pi r^3 f(r) \tag{5}$$

and f(r) is the size distribution obtained through either the log-normal fit or the inversion. However, the following discussion of the inversion results will be based on the number density distribution of Figures 6 through 10.

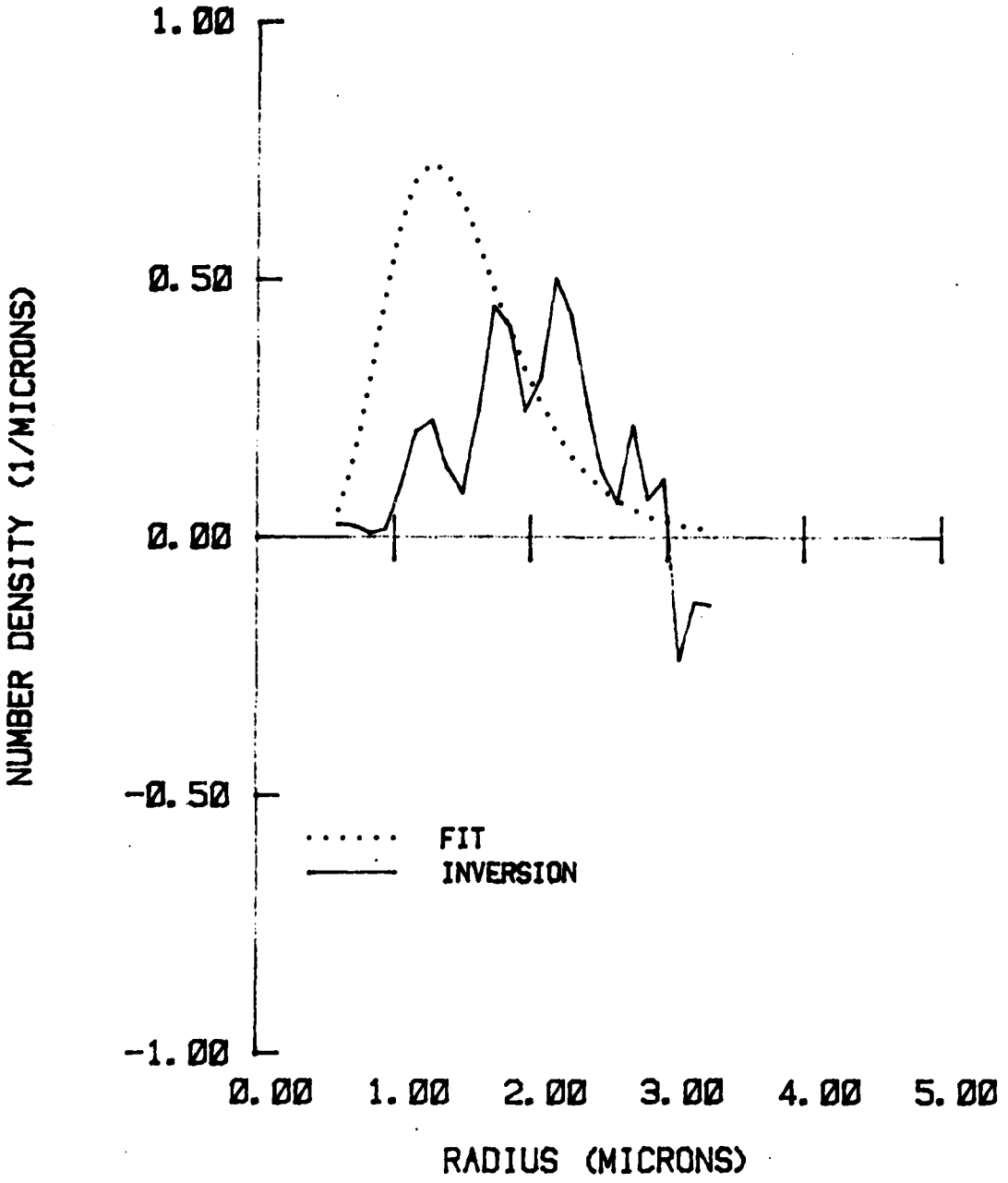

Figure 6. Size Distribution for Set A

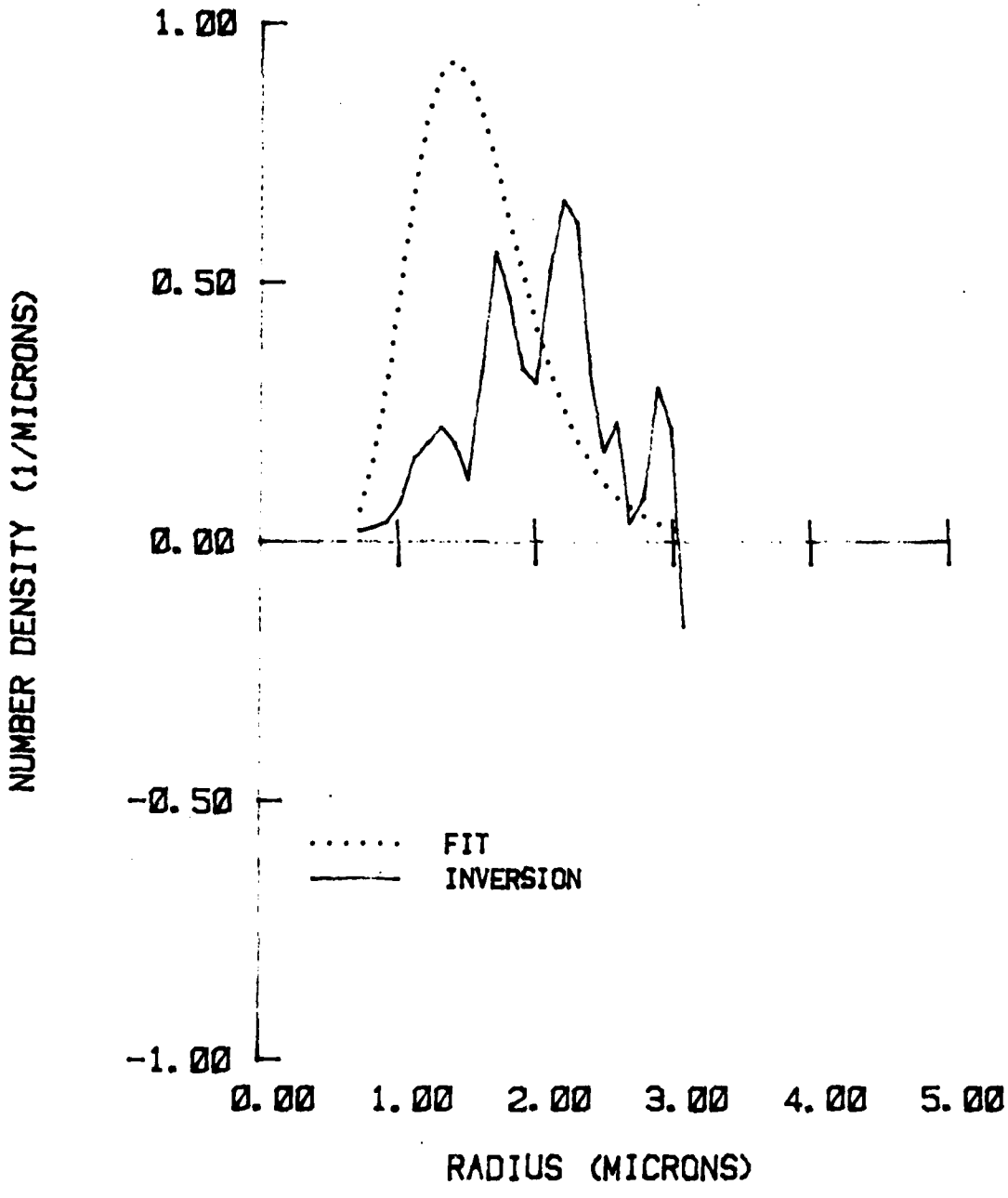

Figure 7. Size Distribution for Set B

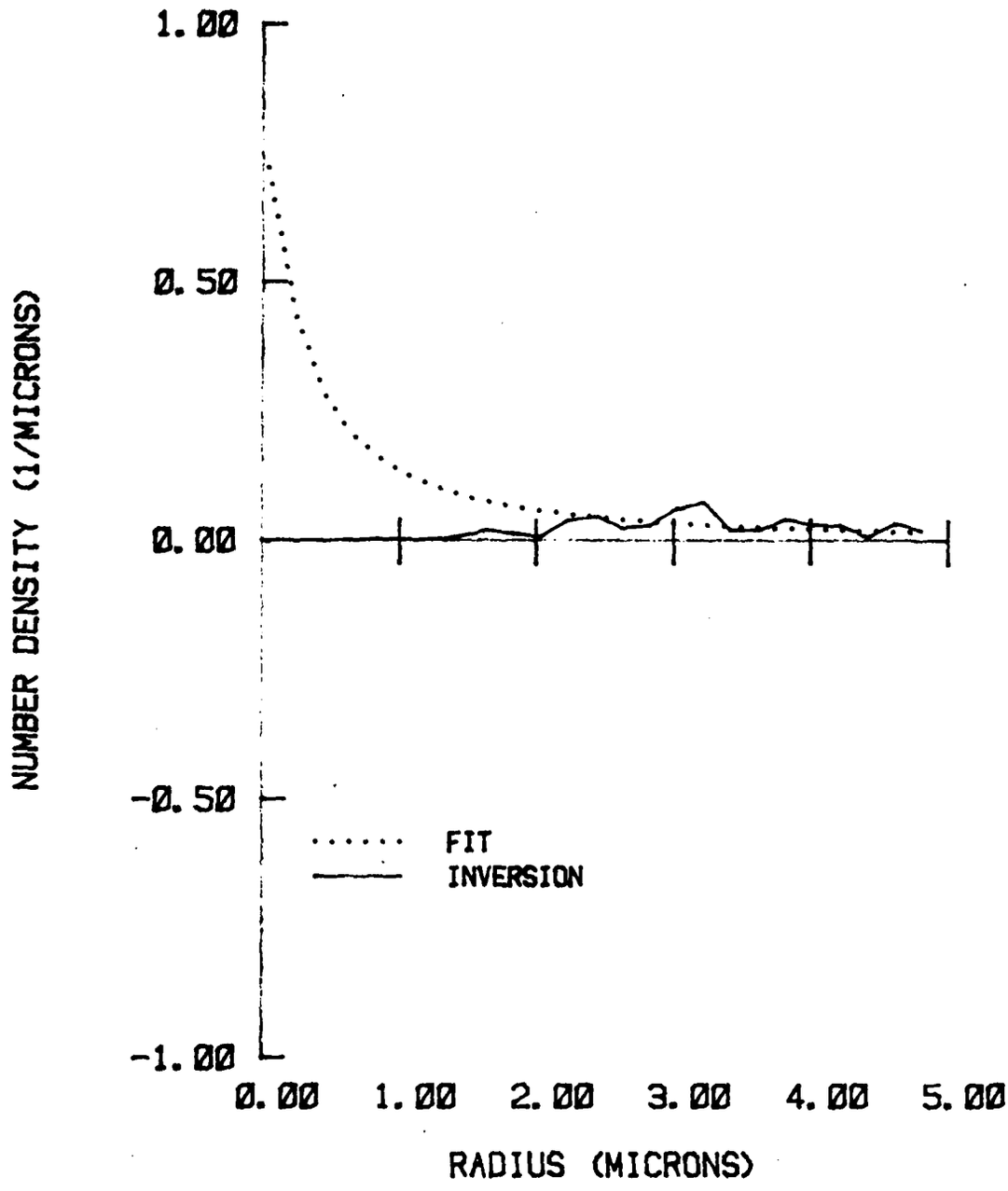

Figure 8. Size Distribution for Set C

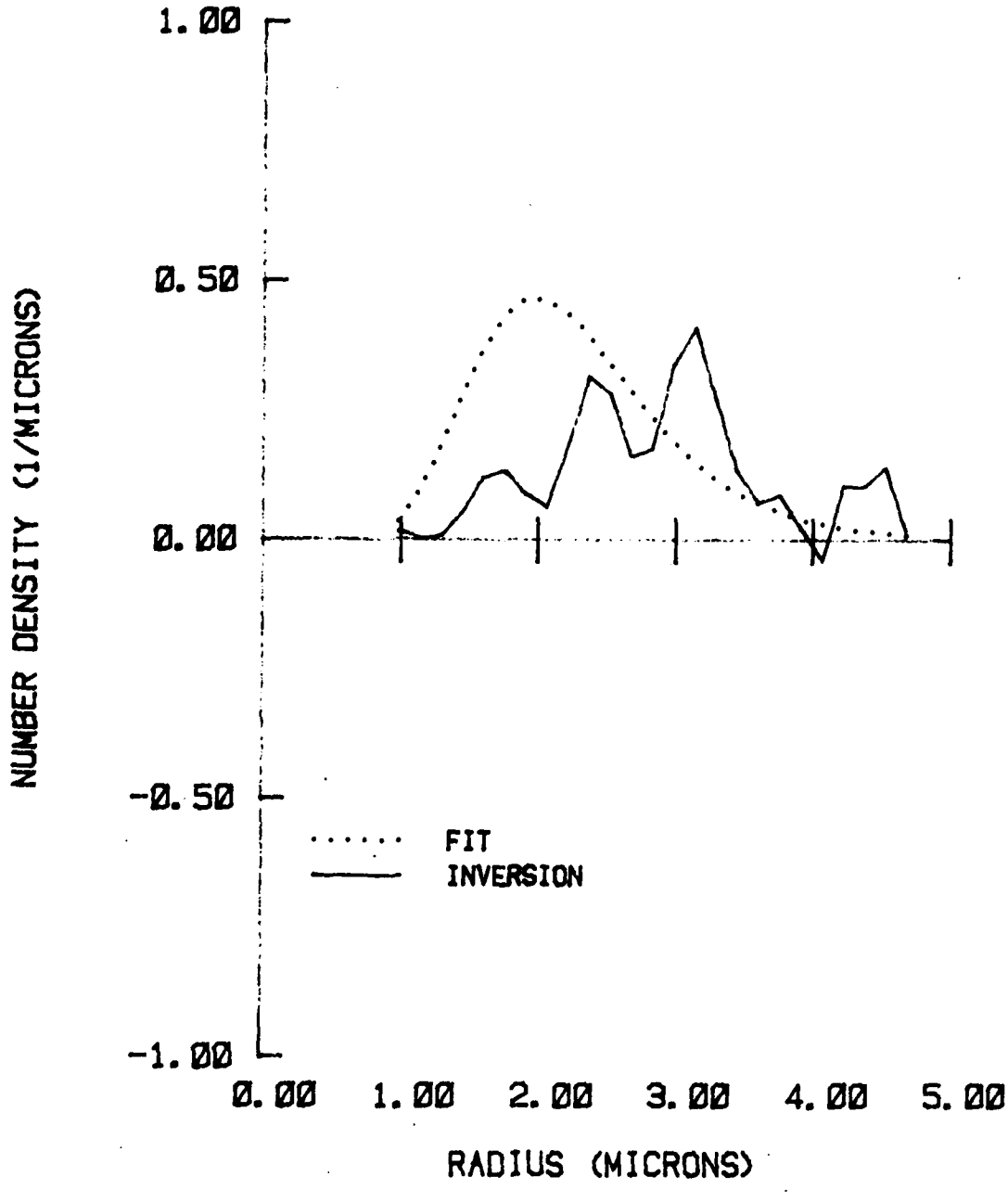

Figure 9. Size Distribution for Set D

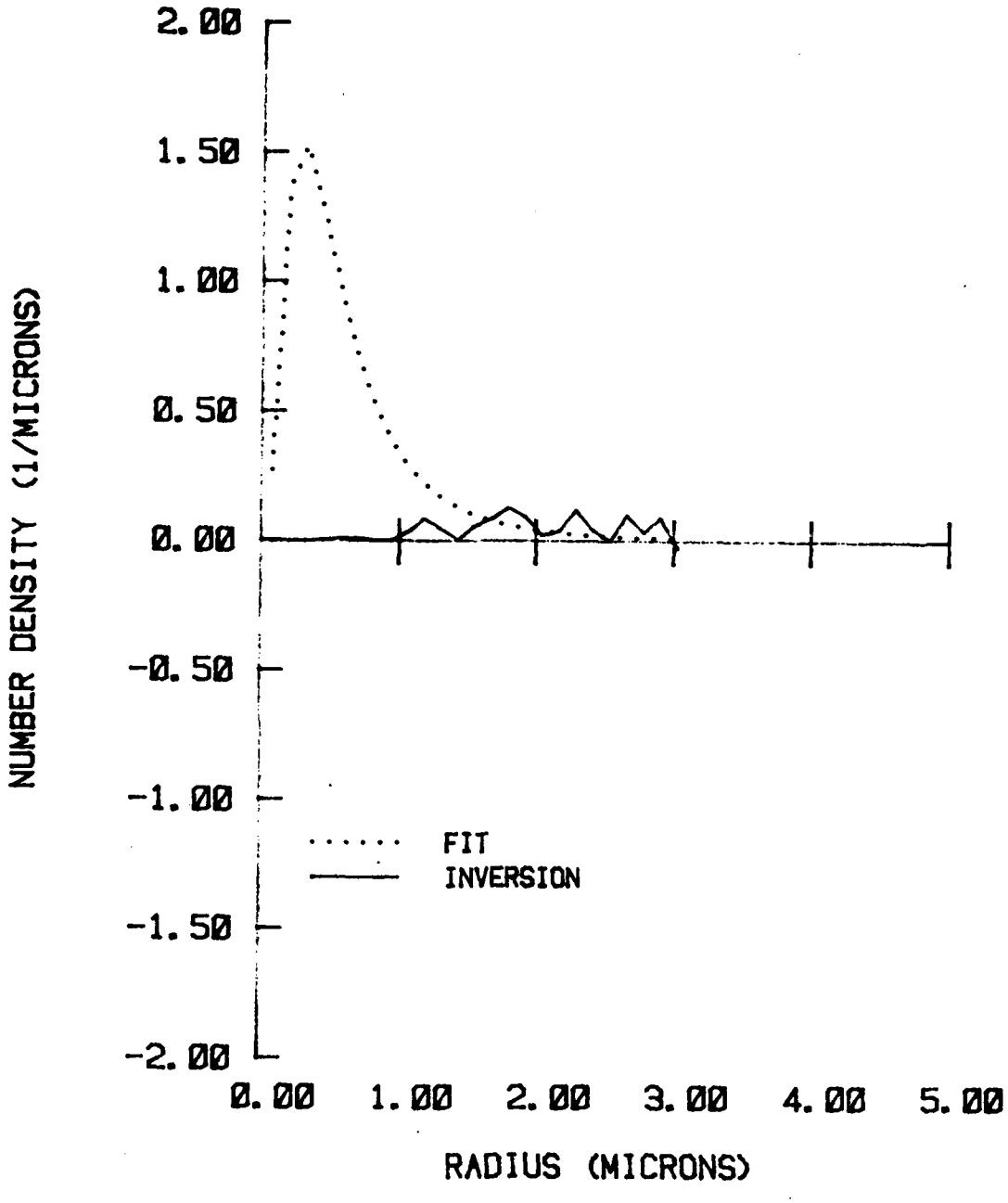

Figure 10. Size Distribution for Set E

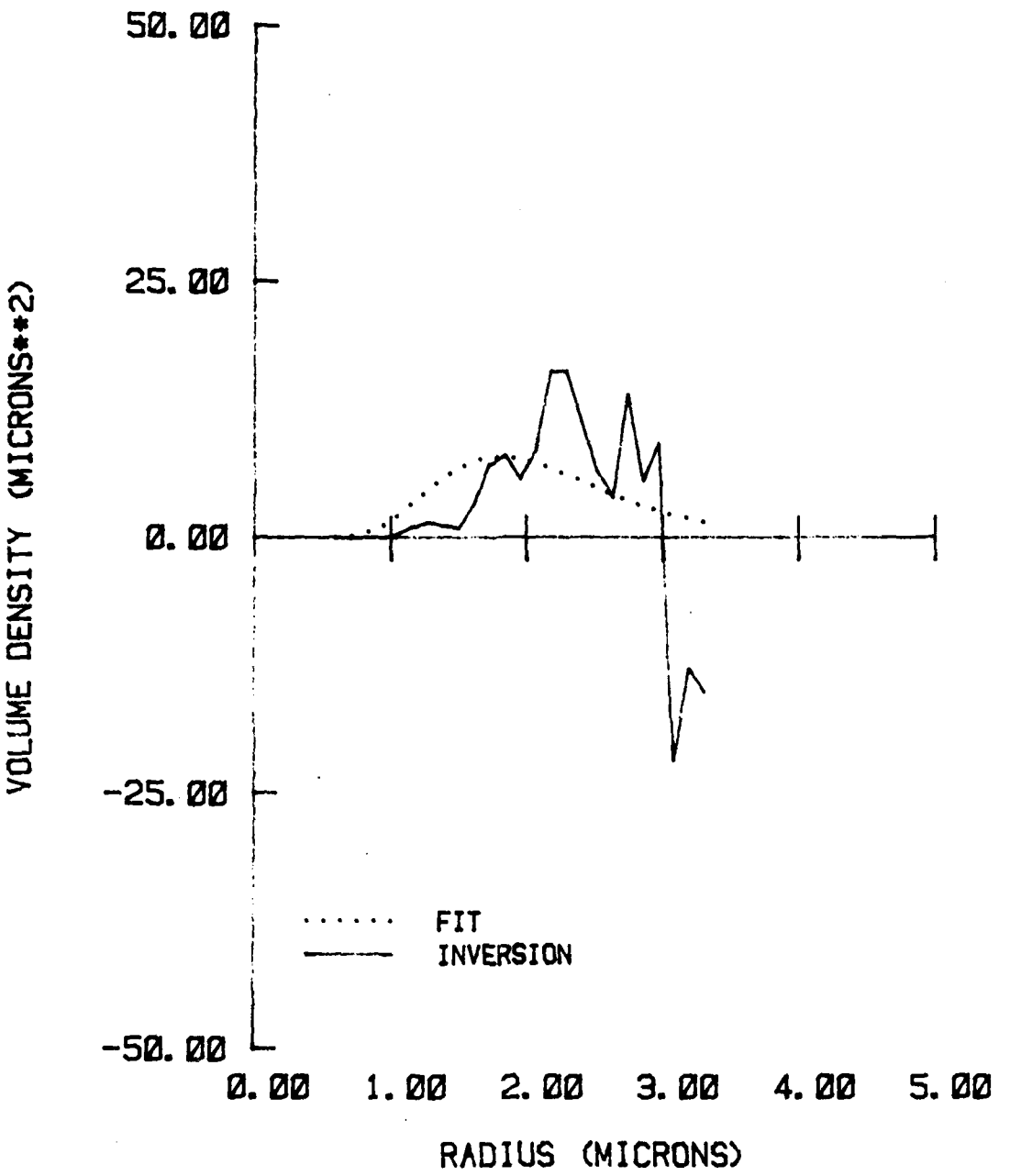

Figure 11. Volume Distribution for Set A

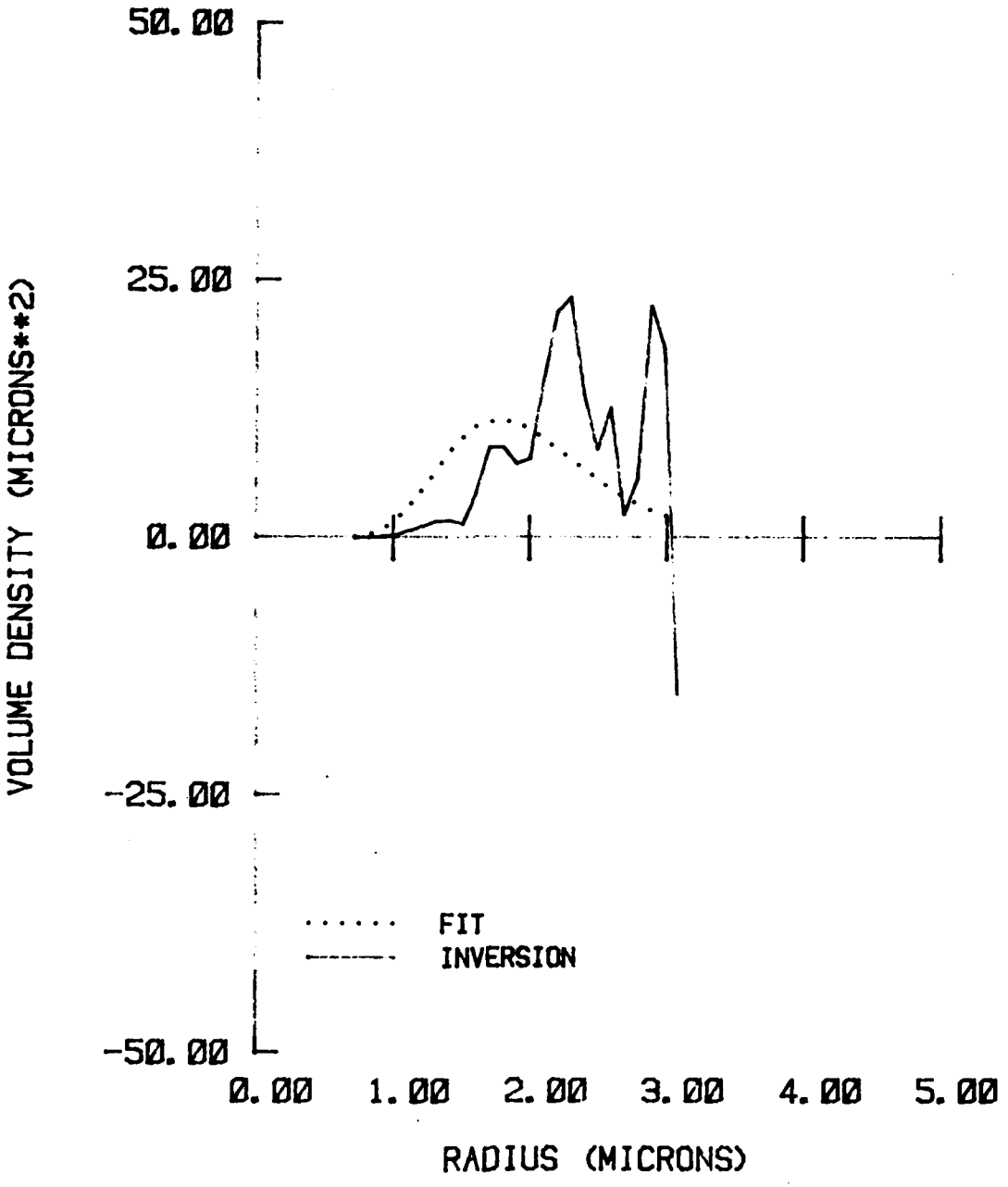

Figure 12. Volume Distribution for Set B

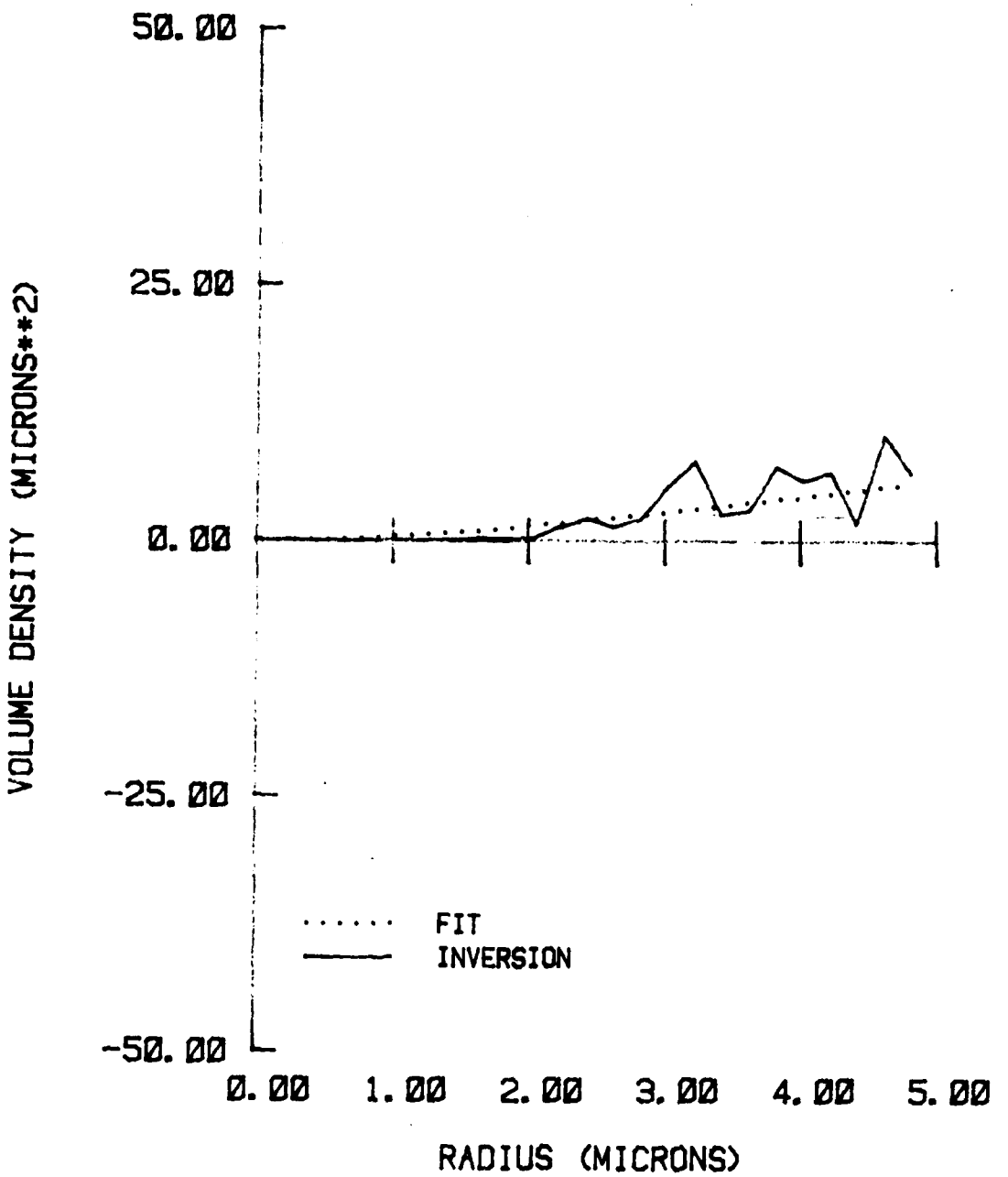

Figure 13. Volume Distribution for Set C

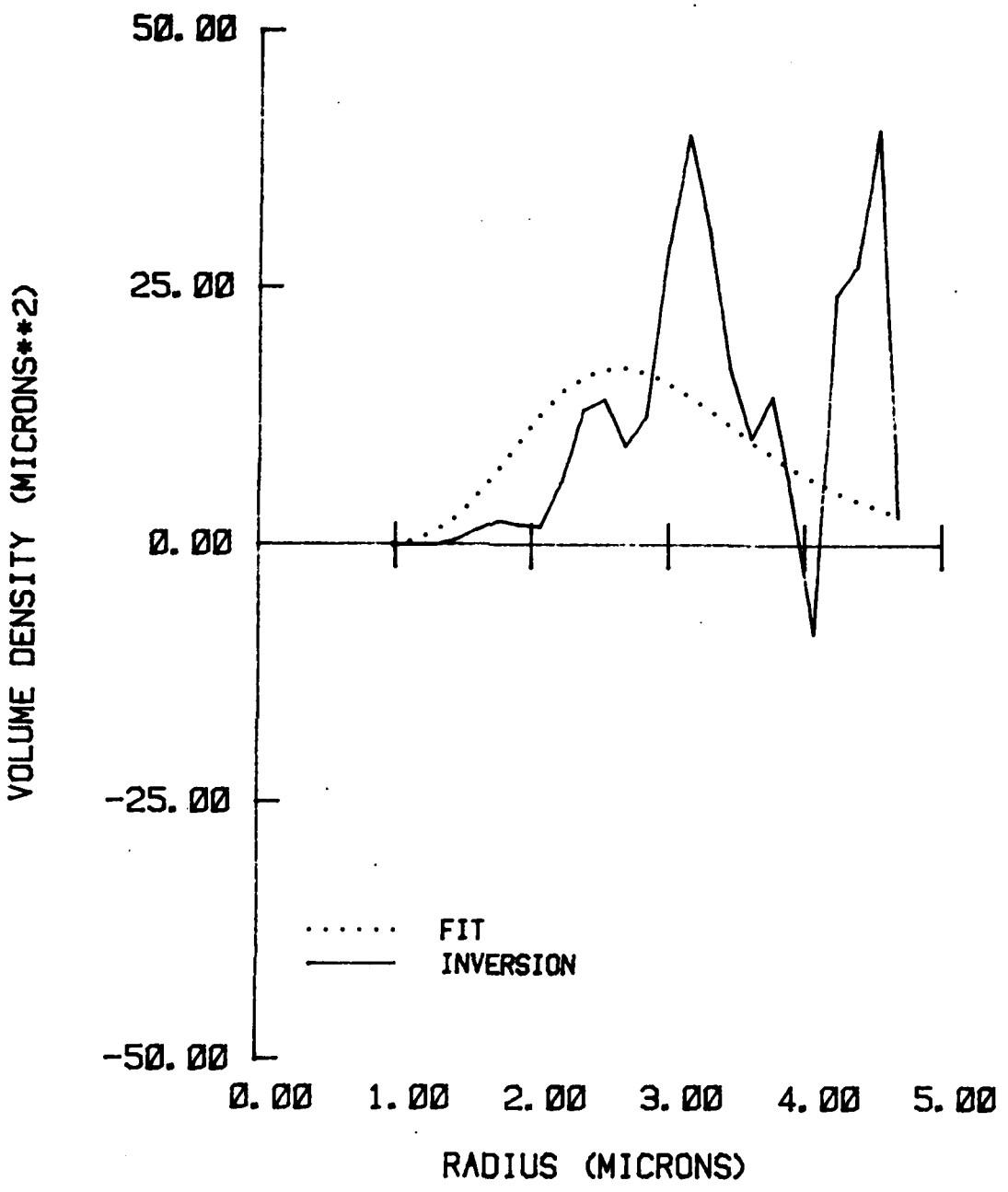

Figure 14. Volume Distribution for Set D

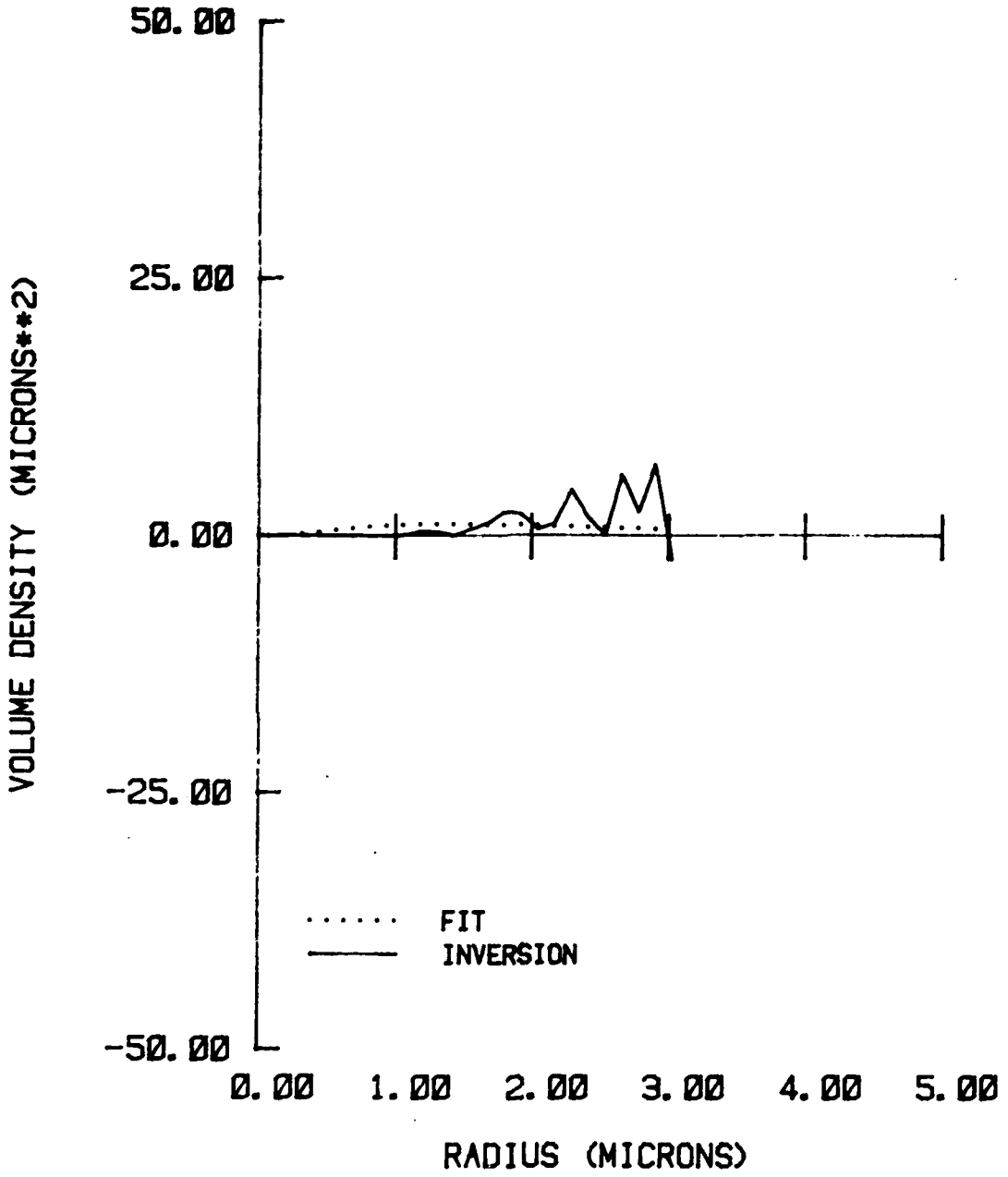

Figure 15. Volume Distribution for Set E

The most consistent feature of the five plots is that the inversion result tends to follow the fit in the upper half of the radius range and tends toward zero in the lower half. This is the expected result, as discussed earlier, since the eigen functions from which the solution must be constructed all tend to zero in this lower radius region. In Sets A, B, and D, where the fit shows significant values in the upper radius region, the inversion is also substantially different from zero and oscillates near the fit value. The size distribution is skewed sharply toward small radius in Sets C and E. In these cases the inversion as well as the fit remains small in the upper radius region.

How much confidence can be placed in the results shown in Figures 6 through 10 The chi-square function, Equation 3, may be used to evaluate the goodness of the log-normal fit. Values of chi-square and the associated confidence level, the probability that chi-square has the given or larger value through a random fluctuation, is given in Table 6. If the confidence level is less than 5% the fit is customarily rejected, i.e. the data is not from the distribution tested. By this criterion Sets A, C, D, and E are not drawn from a simple log-normal distribution. It is interesting to note that the only case for which the fit could not be rejected was Set B which had a larger uncertainty than the others, 10% versus 3%. While the exact form of the distribution is not log-normal the range of sizes should be valid as the fitted distribution and real one must have their major contribution in the same region. Supporting evidence for this comes from the inversion results which make no assumption regarding the form of the distribution. In the upper part of the radius range, the only place the Mie kernels contain reliable information, the fit and inversion results tend to agree.

Table 6. Chi-square Confidence Levels

Set	Chi-Square	Confidence Level
A	23.6	.03
B	14.3	.3
C	32.1	10^{-3}
C	34.1	5×10^{-4}
E	110	10-8

From results of the direct inversion method it is obvious that the Mie kernels contain little information in the lower half of the radius region. The information contained in the data must be supplemented with assumptions about the function in order to obtain a useful inversion. One approach is to use an inversion method such as constrained linear inversion[4] which incorporates a smoothing constraint as a basic part of the algorithm. However, this method, along with others, inextricably mixes the effects of the data and constraints. A new method, based on an extension of the analytic inversion technique, which allows introduction of constraints and separates the contributions of the data and constraints is presented in the following section.

5. EXTENSION OF ANALYTIC INVERSION TECHNIQUE TO INCORPORATE CONSTRAINTS

In a previous paper[2] an analytic inversion technique was developed for Fredholm type remote-sensing problems. A principal result of this work was that only that portion of the solution lying in the space spanned by the kernels could be determined from the data. Often, however, there exists additional knowledge about the solution that could be used. For example, if the solution is a particle size distribution then it must be non-negative. Some other inversion methods, such as constrained linear inversion[4] and the method of Landweber,[5] make use of a smoothing constraint. However, the effects of the data and the constraint are so entangled that it is not possible to separate their individual influences on the solution. The present work will show how it is possible by using the analytic method and a general assumption about the nature of the solution to apply a constraint to obtain the portion of the solution in the space orthogonal to the space spanned by the kernels. As the two parts of the result (the one determined by the data and the other by the constraint) are independent, their relative contributions can be studied.

The assumption referred to in the preceding paragraph is that the solution function can be expressed to the necessary accuracy by a finite Fourier series. In practice, this is not an unreasonable assumption as the

number of terms may be chosen large enough that a conjectured solution can be represented to a desired accuracy.

We will consider the problem of finding a solution to the system of Fredholm integral equations

$$g_i = \int_C^{C+2L} K_i(x)\, f(x)\, dx + e_i \qquad i = 1,2, \ldots . N . \tag{6}$$

The kernels $K_i(x)$ are known functions representing the physical interaction, the g_i are the experimental measurements, the e_i are random experimental errors, and $f(x)$ is the unknown function, assumed to have a finite Fourier series representation. Results regarding the analytic inversion portion of the problem will be taken from the remote sensing data.[2] The following section will establish terminology and notation.

Let V be the vector space over the reals consisting of continuous, real-valued functions on the interval $C \leq x \leq C + 2L$ and the inner product on V be

$$\langle t,u \rangle = \int_C^{C+2L} t(x)\, u(x)\, dx \qquad t, u \in V \tag{7}$$

The norm $||u||$ of a function $u(x)$ is then

$$||u|| = \langle u,u \rangle^{1/2} \tag{8}$$

The finite Fourier series representation of $f(x)$ on the interval $C \leq x \leq C + 2L$ is given by the series

$$f(x) = \frac{c_0}{2} + \sum_{m=1}^{M} \left(c_m \cos \frac{m\pi x}{L} + d_m \sin \frac{m\pi x}{L}\right) \tag{9}$$

with unknown coefficients. The kernels $K_i(x)$ may be represented on the same interval by the Fourier series

$$K_i(x) = \frac{a_{io}}{2} + \sum_{m=1}^{\infty} \left(a_{im} \cos \frac{m\pi x}{L} + b_{im} \sin \frac{m\pi x}{L}\right) \tag{10}$$

where

$$a_{im} = \frac{1}{L} \int_{C}^{C+2L} K_i(x) \cos \frac{m\pi x}{L} \, dx \tag{11}$$

$$b_{im} = \frac{1}{L} \int_{C}^{C+2L} K_i(x) \sin \frac{m\pi x}{L} \, dx \tag{12}$$

Neglecting for the moment the experimental errors we have from equation (6) by a straightforward calculation.

$$g_i = \langle K_i, f \rangle$$

$$= L\left[\frac{a_{io}\, c_o}{2} + \sum_{m=1}^{M} \left(a_{im}\, c_m + b_{im}\, d_m\right)\right] \tag{13}$$

Thus, the values g_i are determined only from the Fourier coefficients of the kernels a_{im} and b_{im} with $m \leq M$. We will define a set of truncated kernels $K_i^T(x)$ by

$$K_i^T(x) = \frac{a_{io}}{2} + \sum_{m=1}^{M} \left(a_{im} \cos \frac{m\pi x}{L} + b_{im} \sin \frac{m\pi x}{L}\right) \tag{14}$$

where a_{im} and b_{im} are given by equations (11) and (12).

From equation (13) we have

$$g_i = \langle K_i, f \rangle = \langle K_i^T, f \rangle \tag{15}$$

which can be normalized to give

$$g_i' = \langle K_i', f \rangle \text{ and } \langle K_i', K_i' \rangle = 1 \tag{16}$$

where

$$g_i' = g_i / ||K_i^T||$$

$$K_i'(x) = K_i^T(x) / ||K_i^T|| \tag{17}$$

$$a_{im}' = a_{im} / ||K_i^T||$$

$$b_{im}' = b_{im} / ||K_i^T||$$

$$||K_i^T||^2 = L \left[\frac{a_{io}^2}{2} + \sum_{m=1}^{M} (a_{im}^2 + b_{im}^2) \right] .$$

The sine and cosine function appearing in the Fourier series are orthogonal elements of V. It is, therefore, possible to construct a 2M+1 dimensional, orthonormal basis for a subspace V' of V from the functions in the Fourier series of equations (9) and (14). We shall express this basis **B** in matrix notation.

$$\mathbf{B}(x) = \frac{1}{\sqrt{L}} \begin{pmatrix} \frac{1}{2} \\ \vdots \\ \cos \frac{m\pi x}{L} \\ \vdots \\ \cos \frac{M\pi x}{L} \\ \vdots \\ \sin \frac{m\pi x}{L} \\ \vdots \\ \sin \frac{M\pi x}{L} \end{pmatrix} \tag{18}$$

any element $u(x)$ of V' can be expressed as

$$u(x) = \mathbf{U}^* \mathbf{B}(x) \tag{19}$$

where $\mathbf{U}$ is a column matrix with $2M+1$ real elements and the asterisk denotes matrix transposition. The elements of $\mathbf{U}$ for a Fourier series expansion, such as equation (9), are given by the relationship

$$\mathbf{U} = \sqrt{L} \begin{pmatrix} \frac{a_0}{\sqrt{2}} \\ a_1 \\ \vdots \\ a_M \\ b_1 \\ \vdots \\ b_M \end{pmatrix} \tag{20}$$

Thus, $f(x)$ and $K_i'(x)$ are elements of V'.

Combining equations (13) and (14) we obtain the normal expression for the scalar product of two vectors in an orthonormal basis

$$\langle t,u \rangle = \sum_{j=1}^{2M+1} t_j \, u_j \qquad t, u \in V' \tag{21}$$

If W is the subspace of V' spanned by the $K_i'(x)$ and X is the orthogonal complement of W in V', the function f(x) can be written

$$f(x) = r(x) + s(x) \qquad r(x) \in W,\ s(x) \in X. \tag{22}$$

From the definition of the orthogonal complement

$$\begin{aligned} g_i' &= \langle K_i', r + s \rangle \\ &= \langle K_i', r \rangle. \end{aligned} \tag{23}$$

An orthonormal basis **P**(x) for W can be constructed from an eigenanalysis of the covariance matrix **C** where

$$C_{ij} = \langle K_i', K_j' \rangle \tag{24}$$

Let p_i be the eigenvalues of **C** arranged in decreasing order, i.e., $p_1 \geq p_2 \geq \ldots \geq p_N$, **U** = matrix whose columns are the unit normalized eigenvectors of **C** arranged in the same order as the eigenvalues, i.e., column 1 is the eigenvector whose eigenvalue is p_1, and

$$\mathbf{A} = \begin{pmatrix} p_1^{-1/2} & & & 0 \\ & p_2^{-1/2} & & \\ & & \ddots & \\ 0 & & & p_N^{-1/2} \end{pmatrix} \tag{25}$$

If $\mathbf{K}'(x)$ is the column matrix whose elements are the functions $K_i'(x)$ an orthonormal basis for W is given by

$$\mathbf{P}(x) = \mathbf{A}\,\mathbf{U}^*\,\mathbf{K}'(x) \tag{26}$$

The matrix $\mathbf{K}'(x)$ can be expressed in terms of the basis $\mathbf{B}(x)$ by

$$\mathbf{K}'(x) = \mathbf{F}^*\,\mathbf{B}(x) \tag{27}$$

where F is the (2M+1) x N matrix whose i^{th} column is given in terms of the Fourier expansion coefficients of $K_i'(x)$ by equation (20). Equations (26) and (27) lead immediately to the expression of the basis $\mathbf{P}(x)$ of W in terms of the basis $\mathbf{B}(x)$ of V'.

$$\mathbf{P}(x) = \mathbf{R}\,\mathbf{B}(x) \tag{28}$$

where

$$\mathbf{R} = \mathbf{A}\,\mathbf{U}^*\,\mathbf{F}^* \tag{29}$$

The solution to equation (23) is

$$\begin{aligned} r(x) &= \mathbf{E}^*\,\mathbf{P}(x) \\ &= \mathbf{E}^*\,\mathbf{R}\,\mathbf{B}(x) \end{aligned} \tag{30}$$

where

$$\mathbf{E} = \mathbf{A}\,\mathbf{U}^*\,\mathbf{G}' \tag{31}$$

$\mathbf{G}'$ being the column matrix whose elements are the g_i'. The highest index elements of the N x 1 matrix E may be set equal to zero depending on the uncertainties e_i of equation (6) and the error analysis.[1]

Throughout the above derivation it has been assumed that there were N eigenvectors of the covariance matrix **C**. However, if some of the $K_i(x)$ are linear combinations of the others then there will be N' < N eigenvectors. The above results are valid with the appropriate changes of dimensionality. In the remainder of the paper we shall use N' as the dimension of W to reflect the fact that it may differ from N, the number of equations in (6).

An analytic expression has been given for r(x), that part of the solution f(x) lying in W. However, as seen from equation (23) s(x), the portion of f(x) in the orthogonal space X, is independent of the data. This means that additional information must be applied to the problem in order to determine s(x). Often, other information is available. For example, if f(x) is a probability density function then it must be non-negative.

The first step to finding s(x) is to construct an orthonormal basis **Q**(x) for X. This can easily be done as the basis **B**(x) of V' and the basis **P**(x) of the orthogonal complement of X in V' are known. The dimensionality of **Q**(x) is M' = (2M+1) - N'.

Let

$$\mathbf{Q}(x) = \mathbf{S}\,\mathbf{B}(x) \tag{32}$$

where **S** is an M' x (2M+1) coefficient matrix to be determined. The requirement that the spaces W and X be orthogonal complements can be expressed as

$$\langle P_i, Q_j \rangle = 0 \qquad i = 1, \ldots, N',\ j = 1, \ldots, M' \tag{33}$$

Starting with j = 1 equation (33, provides N' equations of the form

$$\sum_{m=1}^{2M+1} R_{im}\, S_{1m} = 0 \tag{34}$$

These may be solved by setting (2M+1) - N' of the S_{1m} equal to an arbitrary constant and solving the N' linear equation for the N' remaining coefficients.

The normalization can then be determined by the requirement $\langle Q_j, Q_j \rangle = 1$. This procedure can be iterated to find the next set of S_{jm} where, in addition to the N' equation of the form of equation (34), there are the j' equations of orthogonality in X

$$\sum_{m=1}^{2M+1} S_{jm} S_{j'm} = 0, \qquad j' < j. \tag{35}$$

Thus, the matrix **S** can be constructed by a well-defined, iterative procedure from **R**.

The solution f(x) to equation (1) can now be expressed as

$$f(x) = \mathbf{E}^* \mathbf{P}(x) + \mathbf{H}^* \mathbf{Q}(x) \tag{36}$$

where **H** is the M' x 1 matrix of unknown coefficients to be determined by the constraint. A computationally efficient representation of f(x) is

$$f(x) = (\mathbf{E}^* \mathbf{R} + \mathbf{H}^* \mathbf{S})\, \mathbf{B}(x). \tag{37}$$

The matrix **H** may now be determined by applying the constraint to f(x) as all other quantities appearing in equation (37) are known. This would commonly be accomplished by creating an evaluation function from f(x) incorporating the constraint conditions and using a numerical minimizing algorithm to determine the elements of **H**.

A convenient measure of the effect of the constraints on the solution is given by the ratio R of the norms of f(x) and s(x).

$$R = \frac{||s||}{||f||} = \left[\sum_{m=1}^{M'} H_m^2\right]^{1/2} \left[\sum_{i=1}^{N'} E_i^2 + \sum_{m=1}^{M'} H_m^2\right]^{-1/2} \tag{38}$$

The solution f(x) to equation (6) has now been found as the sum of two independent terms, one depending on the data and the other on the constraints. These two, r(x) and s(x), can be studied individually to understand the relative importance of the data and constraints to the solution.

6. RECOMMENDATIONS

The preceeding work shows there are two areas where additional research is needed:

1) A wider search should be made for an optimal set of measurements. This search would use a larger number of combinations of wavelengths, angles, and polarization in an attempt to find more than the 12 independent pieces of information that constitute the present optimal set.

2) The theory, presented in Section 5, which allows constraints to be added to the analytic inversion technique should be programmed. Different constraints such as requiring a non-negative solution, first or second derivative smoothing, and minimum deviation should be tried and tested against data of the type used in this report.

The research program should provide a better set of experimental measurements to characterize particle size distribution and a better inversion method. This method would contain both the smoothing effects of constraints and the analytic dependence on data and would show the quantitative contributions of each.

Blank

LITERATURE CITED

1. Henning, R. L., Capps, C D., Hess, G. M. Inversion Technique Evaluation. Report No. ARCSL-CR-82047. October 1982. Boeing Aerospace Company. Seattle, WA. UNCLASSIFIED Report.

2. Capps, C. D., Henning, R. L., Hess, G. M. Analytic Inversion of Remote-Sensing Data. Applied Optics 21, 3581 (1982).

3. Marquardt, D. W. An Algorithm for Heart-Squares Estimation of Nonlinear Parameters. J. SIAM 11, 2 (1963).

4. Twomey, S. Introduction to the Mathematics of Inversion in Remote Sensing and Indirect Measurements. (Elsevier, New York, 1977).

5. Landweber, L. Am. J. Mth. 73, 615 (1951).

Blank

DISTRIBUTION LIST 9

Names	Copies
CHEMICAL RESEARCH AND DEVELOPMENT CENTER	
ATTN: DRSMC-CLB (A)	1
ATTN: DRSMC-CLB-C (A)	1
ATTN: DRSMC-CLB-R (A)	1
ATTN: DRSMC-CLB-R(M) (A)	1
ATTN: DRSMC-CLC-B (A)	1
ATTN: DRSMC-CLC-C (A)	1
ATTN: DRSMC-CLC-E (A)	1
ATTN: DRSMC-CLF (A)	1
ATTN: DRSMC-CLJ-IL (A)	2
ATTN: DRSMC-CLJ-IR (A)	1
ATTN: DRSMC-CLJ-M (A)	1
ATTN: DRSMC-CLJ-P (A)	1
ATTN: DRSMC-CLT (A)	1
ATTN: DRSMC-CLW-C (A)	1
ATTN: DRSMC-CLY-A (A)	1
ATTN: DRSMC-CLR-I (A)	1
ATTN: DRSMC-CLY-R (A)	10
COPIES FOR AUTHOR(S)	
ATTN: DRSMC-CLB-PS (A) (Dr.Bottiger - COR)	20
RECORD COPY: DRSMC-CLC-A (A)	1
DEPARTMENT OF DEFENSE	
Defense Technical Information Center ATTN: DTIC-DDA-2 Cameron Station, Building 5 Alexandria, VA 22314	12
Director Defense Intelligence Agency ATTN: DB-4G1 Washington, DC 20301	1
Commander USASED, USAINSCOM ATTN: IAFM-SED-III Fort Meade, MD 20755	1
DEPARTMENT OF THE ARMY	
HQDA ATTN: DAMO-NCC WASH DC 20310	1
Federal Emergency Management Agency Office of Research/NPP ATTN: David W. Bensen Washington, DC 20472	1
HQ DA (DAMA-CSS-C) Washington, DC 20310	1
HQ Sixth US Army ATTN: AFKC-OP-NBC Presidio of San Francisco, CA 94129	1
Commander DARCOM, STITEUR ATTN: DRXST-STI Box 48, APO New York 09710	1
Commander USASTCFEO ATTN: MAJ Mikeworth APO San Francisco 96328	1
HQ, 5th Infantry Division (Mech) ATTN: Division Chemical Officer Fort Polk, LA 71459	1
Army Research Office ATTN: DRXRO-CB (Dr. R. Ghirardelli) P.O. Box 12211 Research Triangle Park, NC 27709	1

OFFICE OF THE SURGEON GENERAL

Commander
US Army Medical Bioengineering Research
and Development Laboratory
ATTN: SGRD-UBD-AL, Bldg 568 1
Fort Detrick, Frederick, MD 21701

Commander
USA Medical Research Institute of
Chemical Defense
ATTN: SGRD-UV-L 1
Aberdeen Proving Ground, MD 21010

Commander
US Army Environmental Hygiene Agency
ATTN: HSHB-O (B. Donovan) 1
Aberdeen Proving Ground, MD 21010

US ARMY MATERIEL DEVELOPMENT AND
READINESS COMMAND

Commander
HQ, DARCOM
ATTN: DRCED (BG Robinson) 1
5001 Eisenhower Ave
Alexandria, VA 22333

Commander
US Army Materiel Development and
Readiness Command
ATTN: DRCSF-P 1
5001 Eisenhower Ave
Alexandria, VA 22333

Director
Human Engineering Laboratory
ATTN: DRXHE-IS (Barnes) 1
Aberdeen Proving Ground, MD 21005

Commander
US Army Foreign Science & Technology Center
ATTN: DRXST-MT3 1
220 Seventh St., NE
Charlottesville, VA 22901

Director
US Army Materiel Systems Analysis Activity
ATTN: DRXSY-MP 1
ATTN: DRXSY-CR (Mr. Metz) 1
Aberdeen Proving Ground, MD 21005

Commander
US Army Missile Command
Redstone Scientific Information Center
ATTN: DRSMI-RPR (Documents) 1
Redstone Arsenal, AL 35898

Director
DARCOM Field Safety Activity
ATTN: DRXOS-C 1
Charlestown, IN 47111

Commander
US Army Natick Research and Development
Laboratories
ATTN: DRDNA-O 1
ATTN: DRDNA-IC 1
Natick, MA 01760

US ARMY ARMAMENT, MUNITIONS AND
CHEMICAL COMMAND

Commander
US Army Armament, Munitions and
Chemical Command
ATTN: DRSMC-ASN (R) 1
ATTN: DRSMC-IRW (R) 1
ATTN: DRSMC-SF (R) 1
Rock Island, IL 61299

Commander
USA AMCCOM
ATTN: SMCTE 1
Aberdeen Proving Ground, MD 21010

Commander
US Army Dugway Proving Ground
ATTN: Technical Library (Docu Sect) 1
Dugway, UT 84022

US ARMY ARMAMENT RESEARCH AND DEVELOPMENT CENTER

Commander
US Army Armament Research and Development Center
ATTN: DRSMC-LCA-L (D) 1
ATTN: DRSMC-LCU-CE (D) 1
ATTN: DRSMC-SCM (D) 1
ATTN: DRSMC-SCP (D) 1
ATTN: DRSMC-TDC (D) (Dr. D. Gyorog) 1
ATTN: DRSMC-TSS (D) 2
ATTN: DRCPM-CAWS-AM (D) 1
Dover, NJ 07801

Armament Research and Development Center
USA AMCCOM
ATTN: DRSMC-TSE-OA (D) (Robert Thresher) 1
National Space Technology Laboratories
NSTL Station, MS 39529

Commander
AMCCOM
ATTN: DRSMC-QAC-E (A) 1
Aberdeen Proving Ground, MD 21010

Commander
USA Technical Detachment 1
US Naval EOD Technology Center
Indian Head, MD 20640

US ARMY TRAINING & DOCTRINE COMMAND

Commandant
US Army Infantry School
ATTN: CTDD, CSD, NBC Branch 1
Fort Benning, GA 31905

Commandant
US Army Missile & Munitions Center and School
ATTN: ATSK-TME 1
Redstone Arsenal, AL 35898

Commander
US Army Logistics Center
ATTN: ATCL-MG 1
ATTN: DLSIE 1
Fort Lee, VA 23801

Commandant
US Army Chemical School
ATTN: ATZN-CM-C 1
ATTN: ATZN-CM-AFL 2
ATTN: ATZN-CM-TPC 2
Fort McClellan, AL 36205

Commander
USAAVNC
ATTN: ATZQ-D-MS 1
Fort Rucker, AL 36362

Commander
US Army Infantry Center
ATTN: ATSH-CD-MS-C 1
Fort Benning, GA 31905

Commander
US Army Infantry Center
Directorate of Plans & Training
ATTN: ATZB-DPT-PO-NBC 1
Fort Benning, GA 31905

Commander
USA Training and Doctrine Command
ATTN: ATCD-N 1
Fort Monroe, VA 23651

Commander
US Army Armor Center
ATTN: ATZK-CD-MS 1
ATTN: ATZK-PPT-PO-C 1
Fort Knox, KY 40121

Commander
USA Combined Arms Center and Fort Leavenworth
ATTN: ATZL-CAM-IM 1
Fort Leavenworth, KS 66027

US ARMY TEST & EVALUATION COMMAND

Commander
US Army Test & Evaluation Command
ATTN: DRSTE-CT-T 1
Aberdeen Proving Ground, MD 21005

DEPARTMENT OF THE NAVY

Project Manager
Threatre Nuclear Warfare Project Office
ATTN: PM-23 (Dr. Patton 1
ATTN: TN-09C 1
Navy Department
Washington, DC 20360

Chief of Naval Research
ATTN: Code 441 1
800 N. Quincy Street
Arlington, VA 22217

Officer-in-Charge
Marine Corps Detachment 1
Naval Explosive Ordnance Disposal
Technology Center
Indian Head, MD 20640

Commander
Naval Surface Weapons Center
Code G51 1
Dahlgren, VA 22448

Chief, Bureau of Medicine & Surgery
Department of the Navy
ATTN: MED 3C33 1
Washington, DC 20372

Commander
Naval Air Development Center
ATTN: Code 2012 (Dr. Robert Helmbold) 1
Warminster, PA 18974

US MARINE CORPS

Commanding General
Marine Corps Development and
Education Command
ATTN: Fire Power Division, D091 1
Quantico, VA 22134

DEPARTMENT OF THE AIR FORCE

Department of the Air Force
Headquarters Foreign Technology Division
ATTN: TQTR 1
Wright-Patterson AFB, OH 45433

ASD/AESD 1
Wright-Patterson AFB, OH 45433

AFAMRL/HE
ATTN: Dr. Clyde Repioggie 1
Wright-Patterson AFB, OH 45433

AFAMRL/TS
ATTN: COL Johnson 1
Wright-Patterson AFB, OH 45433

AFWAL/FIEEC (Wendell Banks) 1
Wright-Patterson AFB, OH 45433

HQ, AFSC/SDNE 1
Andrews AFB, MD 20334

HQ, AFSC/SGB 1
Andrews AFB, DC 20334

HQ, NORAD
ATTN: J-3TU 1
Peterson AFB, CO 80914

USAF TAWC/THL 1
Eglin AFB, FL 32542

USAF SC
ATTN: AD/YQ 1
ATTN: AD/YQO (MAJ Owens) 1
Eglin AFB, FL 32542

USAFSAM/VN
Deputy for Chemical Defense
ATTN: Dr. F. Wesley Baumgardner 1
Brooks AFB, TX 78235

AMD/RDTK
ATTN: LTC T. Kingery 1
Brooks AFB, TX 78235

AMD/RDSM 1
Brooks AFB, TX 78235

AMD/RDSX 1
Brooks AFB, TX 78235

AD/XRO 1
Brooks AFB, TX 78235

OUTSIDE AGENCIES

Battelle, Columbus Laboratories
ATTN: TACTEC 1
505 King Avenue
Columbus, OH 43201

Center for Disease Control
ATTN: Logging Control Officer 1
Mrs. M. Brocato (W.L.Webb)
Atlanta, GA 30333

Director
Central Intelligence Agency
ATTN: AMR/ORD/DD/S&T 1
Washington, DC 20505

ADDITIONAL ADDRESSEES

Commandant
Academy of Health Sciences, US Army
ATTN: HSHA-CDH 1
ATTN: HSHA-IPM 1
Fort Sam Houston, TX 78234

Commander
217th Chemical Detachment
ATTN: AFVL-CD 1
Fort Knox, KY 40121

Headquarters
US Army Medical Research and
Development Command
ATTN: SGRD-RMS 1
Fort Detrick, MD 21701

Stimson Library (Documents) 1
Academy of Health Sciences, US Army
Bldg. 2840
Fort Sam Houston, TX 78234

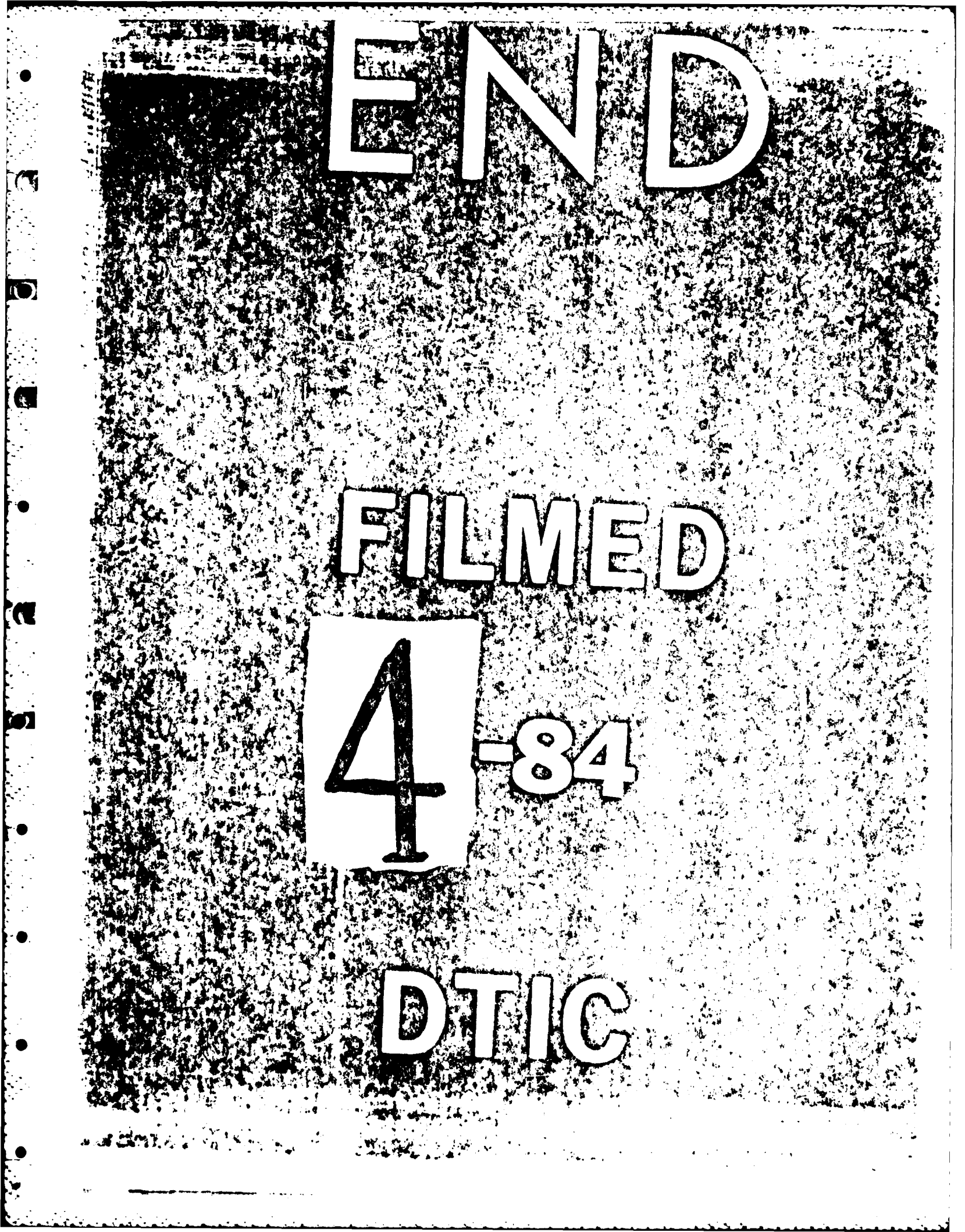
END
FILMED
4-84
DTIC